Nanoscale

Accepted Manuscript

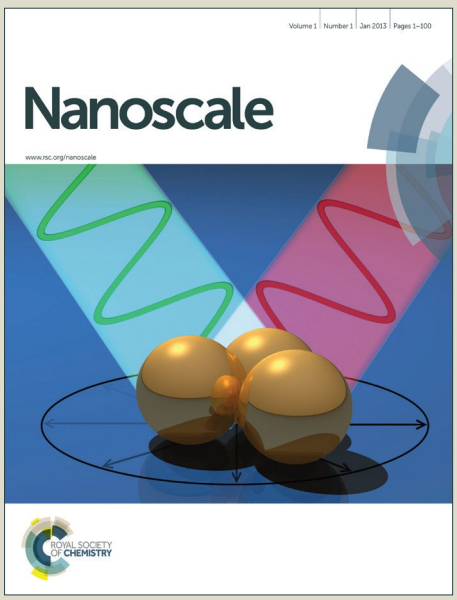

ROYAL SOCIETY OF CHEMISTRY

www.rsc.org/nanoscale

Graphene meta-interface for enhancing the stretchability of brittle oxide layers

Sejeong Won[1,†], Jae-Won Jang[2,†], Hyung-Jin Choi[3], Chang-Hyun Kim[1], Sang Bong Lee[1], Yun Hwangbo[1], Kwang-Seop Kim[1], Soon-Gil Yoon[3], Hak-Joo Lee[1], Jae-Hyun Kim[1,*] and Soon-Bok Lee[2,*]

[1]Department of Nanomechanics, Nano-Convergence Mechanical Systems Research Division, Korea Institute of Machinery & Materials (KIMM), 156 Gajungbuk-ro, Yuseong-gu, Daejeon 305-343, Republic of Korea

[2]Department of Mechanical Engineering, Korea Advanced Institute of Science and Technology (KAIST), 291 Daehak-ro, Yuseong-gu, Daejeon 34141, Republic of Korea

[3]Department of Materials Science and Engineering, Chungnam National University, 99 Daehak-ro, Yuseong-gu, Daejeon 305-764, Republic of Korea

† These authors equally contributed to this work.

* Corresponding authors: jaehkim@kimm.re.kr, sblee@kaist.ac.kr

Table of Contents

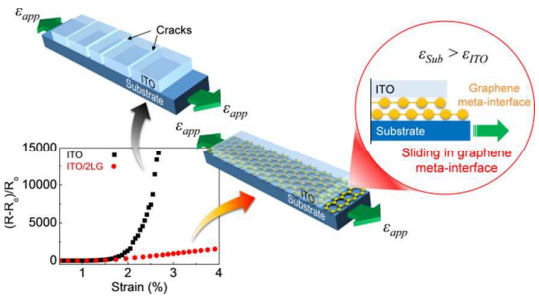

The electromechanical stretchability of brittle oxide layers on polymeric films was enhanced by introducing a graphene meta-interface to reduce the strain transferred from the polymeric film to the oxide

ABSTRACT

Oxide materials have attracted much recent research attention for applications in flexible and stretchable electronics due to their excellent electrical properties and their compatibility with established silicon semiconductor processes. Their widespread uptake has been hindered, however, by the intrinsic brittleness and low stretchability. Here we investigate the use of a graphene meta-interface to enhance the electromechanical stretchability of fragile oxide layers. Electromechanical tensile tests of indium tin oxide (ITO) layers on polymer substrates were carried out with *in situ* observations using an optical microscope. It was found that the graphene meta-interface reduced the strain transfer between the ITO layer and the substrate, and this behavior was well described using a shear lag model. The graphene meta-interface provides a novel pathway for realizing flexible and stretchable electronic applications based on oxide layers.

Keywords: graphene, meta-interface, electromechanical stretchability, oxide materials, *in situ* tensile test, shear lag model

INTRODUCTION

Oxide materials are important for applications as conductors, semiconductors, dielectrics, ferroelectrics and piezoelectrics, and have potential applications in flexible and stretchable electronics because of their excellent electrical properties and wide range of possible material combinations.[1-5] However, the intrinsic brittleness has been an obstacle to their widespread usage in flexible and stretchable electronics.[6, 7] For example, indium tin oxide (ITO) has been the most widely used electronic material for transparent electrodes; however, ITO layers usually fracture even at the small tensile strain of less than 1.4%, and this is accompanied by a rapid degradation of the electrical resistance.[8-10] The electrical functionality of materials degrades under excess strain, and the critical tensile strain above which the required electrical function is lost is defined as the electromechanical stretchability.[11] Much work has been carried out with the aim of increasing the electromechanical stretchability of oxide materials for applications in flexible electronics. One approach is to control the crystalline quality, and hence improve the intrinsic strength.[12] Another is to reduce the density of surface defects via the deposition of an additional layer.[13, 14] A third is to use a passivation layer to reduce the crack driving force or energy release rate in the oxide layer.[15] In addition to these approaches, the use of PDMS adhesive was also proposed to isolate the strain transferred from the unconventional substrates to silicon devices.[16] We are motivated to maintain compatibility with these existing approaches and to further enhance the electromechanical stretchability of oxide materials by engineering the interface with atomic layers between the oxide materials and substrates. This engineered interface is called by meta-interface here, and is superior to a conventional interface between

two adjacent materials in that it can reduce strain transfer between two materials while keeping mechanical contact of them.

Here we propose the use of a graphene meta-interface to improve the stretchability of the oxide layer for applications in flexible electronics. Electromechanical tensile tests of ITO layers on polymer substrates were performed with *in situ* optical microscope observations. The electromechanical stretchability of the ITO layer was increased by inserting a graphene meta-interface between the ITO layer and the substrate. To investigate the mechanism by which the graphene meta-interface improves the electromechanical stretchability, we experimentally measured the electrical resistance and the crack density of the ITO, and the electromechanical behavior of the graphene meta-interface was analyzed using a shear lag model. We find that the main reason of the improved electromechanical stretchability is reduction of the transferred strain from the substrate to the ITO layer due to interlayer sliding in the graphene meta-interface.

RESULT AND DISCUSSION

Tensile tests with *in situ* optical microscope observations. Figure 1(a) shows cross-sectional schematic diagrams of the two types of structure that were fabricated. Polyethylene terephthalate (PET) substrates were used that were 188-μm-thick. In the type-I structures, an ITO layer was directly deposited on the PET substrate using off-axis RF magnetron sputtering at 120°C. In the type-II structures, a multilayer graphene meta-interface was transferred to the PET substrate using a direct transfer method,[17] followed by deposition of the ITO layer using off-axis RF magnetron sputtering. The off-axis RF magnetron sputtering where plasma is not

directed on a target substrate was used to reduce plasma-induced damage on graphene layers as can be seen in Figure S1.[18] The existence of graphene layers after ITO deposition was verified by Raman spectra as shown in Figure S2. The number of the transferred graphene layers was between two and five.

Initial sheet resistances of type-I and type-II structures were 65 ± 3.7 Ω/sq and 61.7 ± 5.7 Ω/sq, respectively. Figure S3 shows transmittances for type-I and type-II structures. Transmittance of type-I is 80.7 ± 0.86 % and those of type-II are degraded as increasing number of graphene layers from 76.6 ± 0.57 % to 72.1 ± 0.69 % at a wavelength of 550 nm. Since the grain structure and roughness of ITO layer are related to its mechanical properties[18, 19], we performed X-ray diffraction (XRD) measurements to compare the microstructure of the ITO layers on PET substrates with and without graphene meta-interface. Figure S4 shows the XRD data of ITO layers on both types of PET substrates. Two peaks of (222) and (400) were observed similarly on both samples. This shows there is no significant change in the microstructures of the ITO deposited on PET with and without graphene meta-interface. AFM investigations were also conducted to study surface topographies of the two types of samples. Figure S5 shows topographies of ITO and ITO/2LG. They had similar topologies and roughness of 14.3 nm and 11.8 nm, respectively.

In situ electromechanical tensile tests were carried out to investigate changes in the electrical resistance and the surface of the ITO layer in response to the applied strain, with no modifications to the damaged samples. This is a significant advantage compared with ex situ tensile tests, in which the samples are investigated after the tests are carried out, and the damage to the sample induced by loading was altered by unloading. Figure 1(b) shows a schematic diagram of the *in situ* electromechanical

tensile testing system. The specimens were formed of rectangular strips that were 2 mm wide and had a gage length of 14 mm.

Figure 1(c) shows the normalized changes in the electrical resistances of the type-I and type-II structures as a function of the applied tensile strain. The electrical resistance of the type-I structure increased rapidly as the strain increased. However, the resistance was finite, even when the cracks propagated across the entire width of ITO layer. This is because the cracked ITO layers typically retain some small volume of conducting material between any two neighboring ITO fragments,[8, 20] and this behavior has been commonly observed for ITO layers on polymer substrates. The electrical resistance of type-II structure changed significantly less than that of the type-I structure for the same applied strain. Furthermore, the gradient of the resistance versus the strain decreased as the number of graphene layers increased.

In addition, to confirm the effect of the graphene meta-interface under repeated loadings, we performed the electromechanical cyclic tests. The tests were conducted under strain control at a frequency of 1 Hz. A mean strain of 1.48 % and a strain amplitude of 0.37 % were chosen by considering the elastic region of the PET substrate. Figure 1(d) shows the normalized electrical resistance variation of type-I and type-II structures with respect to the number of loading cycles. Normalized changes in electrical resistance of type-II structures were smaller than that of type-I structure up to 10,000 cycles and the improvement of the cyclic stability became higher with the increasing number of graphene layers just like the tensile test results.

Figure 1(e) shows optical microscope images of the two types of structure with 3% strain. Cracks occurred in the ITO layer in the form of straight lines perpendicular to the direction of the tensile load. At the initial stage of loading, the cracks were

generated with wide spacing. New cracks then formed between existing generated cracks as the applied strain increased.

To describe the cracking in response to tensile strain, we define the crack density, n as the total length of cracks per unit area; i.e.,[21, 22]

$$n = \frac{l_1 + l_2 + \cdots + l_i}{A}, \quad (1)$$

where l_i is the length of the i^{th} crack in a surface of area A. The crack density was measured as a function of the applied strain by analyzing the optical microscope images obtained *in situ* during the tests. The crack density of the ITO layer in the type-II structures was significantly smaller than that in the type-I structure and, for a given strain, the crack density of the ITO layer in the type-II structures decreased as the number of graphene layers increased as shown in Fig. 1(f). In general, the crack density increased markedly for strains of less than 2.5%, and then grew more slowly as the strain was further increased. The crack density of the ITO layer on the type-II structures was considerably lower than that on the type-I structure, and both the type-I and type-II structures had similar crack onset strains of 1.2–1.3%. Because the electrical properties of the ITO layer on the polymer substrate deteriorate as the generation of cracks, a lower crack density leads to a smaller increase in the electrical resistance. In addition, we obtained experimental results for ITO/1LG where there is no the graphene meta-interface. Figure S6 shows the crack density and normalized electrical resistance for the ITO/1LG as a function of strain. The crack density for ITO/1LG is similar with or a little lower than that of ITO (type-I). The tiny reduction of the crack density can be ascribed to the weakened interface between the PET substrate and the ITO, but is much smaller than those of other type-II structures.

The smaller crack density in the ITO layer of the type-II structure implies a reduction in the transferred strain from the PET substrate to ITO layer. The transfer of strain is related to the interlayer sliding in the graphene meta-interface. The simplest type-II structure was the ITO/two-layer graphene on PET (ITO/2LG), and this was investigated to gain insight into the sliding behavior. Although it is difficult to observe the sliding behavior directly, it is reasonable to assume that sliding occurs mainly at the interface with the lowest adhesion between adjacent layers[23, 24]. There are three interfaces to be considered. The first is between the upper graphene layer and the ITO; the second is between the upper graphene layer and the lower graphene layer; and the third is between the lower graphene layer and the substrate. Figure 2(a) shows optical microscope images of the ITO/2LG structure before and after the tensile test. After the tensile test, flakes of the thin film detached from the PET substrate and curled up due to the residual stress. These detached flakes and the remaining substrate were analyzed using Raman spectroscopy and energy dispersive X-ray spectroscopy (EDS) to identify the weakest interface.

As shown in Figure 2(b), the scanning electron microscope (SEM) image reveals detached flakes, which consisted of In, Sn, O as listed in below table. Figure 2(c) shows Raman spectra of the flakes, the ITO and the SiO_2/Si substrate. These flakes have G and 2D peaks of graphene and this indicates the presence of graphene on the surface of the flakes. This shows that the detached flakes consist of ITO and graphene. Figure 2(d) and Figure 2(e) show topographies and normalized friction force respectively for the remaining area on PET substrate after detachment of the flake. The area from which the flake detached appeared wrinkled, in contrast to the bare PET, and had a significantly smaller frictional force than that on the bare PET.

Because graphene significantly reduces the frictional force on the PET, the low friction implies that graphene remained on the PET in the regions where the flakes detached. From these analyses, we conclude that adhesion between the upper and lower graphene layers was smaller than that at the other two interfaces.

The interaction forces between artificially stacked graphene layers are small[25] and in particular the frictional force between graphene layers is tiny;[26] therefore the adhesion between graphene layers is expected to be weaker than that of the other interfaces, which enables sliding between graphene layers. This is the main mechanism for the reduced crack density in the ITO layer when the graphene meta-interface was present. Figure 2(f) shows a schematic diagram of this behavior of the ITO/2LG structure under tensile loading. The ITO layer with the graphene meta-interface experiences less strain than the PET substrate because of the sliding between the graphene layers.

Shear lag model. Here we use a shear lag model to describe the interlayer sliding of the type-II structure. This model describes stress transfer via interfacial shear stress. Several shear lag models have been reported, including Cox's shear lag model for a fully elastic interface,[27-29] the Kelly–Tyson model for a fully plastic interface,[30, 31] as well as an elastic–plastic shear lag model.[32] The elastic–plastic shear lag model consists of a strained substrate, a relatively soft elastic–plastic interlayer, and a brittle thin film. Here we use the elastic–plastic shear lag model to describe the type-II structure.

Figure 3(a) shows a schematic diagram of the model of the stress distribution around a cracked segment of the ITO layer. The shear stress–strain behavior of

graphene meta-interface is modeled as an elastic-perfectly plastic material. Tensile stress in the ITO layer that results from the transfer of shear stress is maximized in the center of a segment defined by two adjacent cracks. The substrate experiences uniform strain when it is much thicker than the thin film. The crack density n can be expressed as a function of the strain as follows[32] (a detailed derivation is provided in S1).

In the fully elastic case $(x_p > a)$, we have:

$$n(\varepsilon) = \sqrt{\frac{G}{E}}\left[2\sqrt{pq}\cosh^{-1}\left(\frac{1}{1-\frac{\sigma^*}{E\varepsilon}}\right)\right]^{-1}, \quad (2)$$

whereas in the elastic–plastic case $(x_p < a)$, we have:

$$n(\varepsilon) = \frac{G\gamma_p}{2Eq}\left[\left(\frac{\sigma^*}{E}-\varepsilon\right)\cosh\left(sinh^{-1}\left(\frac{\gamma_p\sqrt{\frac{Gp}{Eq}}}{\varepsilon-\frac{\sigma^*}{E}}\right)\right)+\varepsilon+\gamma_p\sqrt{\frac{Gp}{Eq}}sinh^{-1}\left(\frac{\gamma_p\sqrt{\frac{Gp}{Eq}}}{\varepsilon-\frac{\sigma^*}{E}}\right)\right]^{-1}, \quad (3)$$

where G is the shear modulus of graphene layers, γ_p is the plastic onset shear strain of the graphene layers, σ* is the effective tensile strength of the ITO layer, p is the thickness of graphene meta-interface, q is the thickness of ITO layer, ε is the applied strain, and E is the elastic modulus of the ITO layer. Figure 3(b) shows a comparison of the results of the model with the experimental data. The measured parameters are n, q and ε. The thickness of the graphene meta-interface p was obtained by multiplying the thickness of a single layer of graphene by the number of layers that were transferred. The parameters to be fitted using the model are $\gamma_p = \tau_p/G$, G/E and σ*/E.

With the ITO/2LG, the top layer of graphene adhered to the ITO layer, and the bottom layer of graphene adhered to PET substrate. If the bottom layer were well attached to the substrate, the frictional force on the surface of that layer would be

small.[33] This leads to a small shear modulus of for the 2LG, and the fully elastic case can be used to model the ITO/2LG. By contrast, with the ITO/3LG, ITO/4LG, and ITO/5LG systems, there are one or more graphene layers in addition to the top and bottom layers, which will neither adhere to the oxide nor to the PET substrate. These graphene layers are attracted to each other by van der Waals forces, the strength of which increases as the number of layers increases. This leads to a larger shear modulus than with the ITO/2LG. The elastic–plastic shear lag model rather than a fully elastic shear lag model was used to describe the ITO/3LG, ITO/4LG and ITO/5LG samples. Table 1 lists the parameters that were fitted to the shear lag model. We see that excellent agreement was achieved between the experimental data and the shear lag model for the type-II samples with different numbers of graphene sheets, with a coefficient of determination of $R^2 > 0.95$.

Assuming that the Young's modulus of the ITO layer is 116 GPa, the shear modulus of the 2LG will be 430 kPa. The shear modulus of other cases (i.e., 3LG, 4LG, and 5LG) increased from 750 kPa to 1.4 MPa as the number of graphene sheets increased from 3 to 5, and the shear strength was approximately τ_p = 48 MPa. Note that the shear modulus of Bernal stacked graphene is 4.6 GPa.[34, 35] Because the graphene sheets used in this study were artificially stacked on the PET substrate, the crystalline structure of the graphene meta-interface is far from the Bernal stacked graphene (which has a high degree of symmetry and crystallinity). This can explain the smaller shear modulus of the graphene meta-interfaces compared with Bernal stacked graphene.[34-36] Using the fitted parameters, it is possible to design an oxide layer with a graphene meta-interface on the polymeric substrate with a particular electromechanical stretchability.

Electromechanical behavior of ITO in ITO/multilayer Gr structures. Because the graphene has good electrical conductivity, it is obvious that the type-II structure has lower electrical resistance than the type-I structure. To investigate the changes in the electrical resistance of only the ITO layer as a function of the crack density in the type-II structures, we used the relation between the electrical resistance and crack density of the type-I structure shown in Figure 4(a). The electrical resistance increased exponentially as a function of the crack density. This can be explained using a damage model,[37-39] whereby the change in the electrical resistance (i.e., $R(n) = (R-R_o)/R_o$) is given by

$$R(n) = a(e^{bn} - 1), \quad (4)$$

where the fitting constants are a = 3.45 (non-dimensional) and b = 92.42 m, and n is the crack density. The contribution of the graphene meta-interface as an alternative pathway for the electric current can be accounted for by substituting into this equation the crack densities that were measured for the type-II samples. Figure 4(b) shows the electrical resistance of only the ITO layer without the contribution of the graphene to the electrical conductance of the structure. The gradients of the electrical resistance of only the ITO layer as a function of the strain for the type-II structures were much smaller than those of the type-I structure, and the gradients of the electrical resistance of the type-II structures gradually decreased as the number of graphene layers increased.

By combining the shear lag model for n(ε) in Eqs. (2) and (3) with Eq. (4), we obtain the following relation between the normalized electrical resistance of the ITO layer and applied strain in the type-II structure:

$$R(\varepsilon) = a(e^{bn(\varepsilon)} - 1), \quad (5)$$

where n(ε) is the crack density as a function of the applied strain ε, which depends on the number of graphene sheets. As the number of graphene sheets increased, the change in the electrical resistance of the ITO layer as a function of strain became smaller. Using Eq. 5, it is possible to obtain a desired electromechanical stretchability of the oxide layer using the graphene meta-interface.

CONCLUSION

Oxide materials are of particular interest for flexible and stretchable electronics applications because of their excellent electrical properties and compatibility with silicon semiconductor processes. However, the widespread usage of oxide materials for these applications has been hindered by the intrinsic brittleness. Here we proposed a method of enhancing the electromechanical stretchability of oxide materials. An ITO layer was used as the oxide material, and the electromechanical stretchability was enhanced using multiply transferred graphene sheets to form a meta-interface between the ITO layer and the PET substrate. The mechanism of the improved electromechanical stretchability is the reduction of the transferred strain from the PET substrate to the ITO layer due to the sliding of graphene meta-interface. This sliding behavior depended on the number of graphene sheets, and was well described using a shear lag model. The electromechanical model of ITO layer with the graphene meta-interface was described by combining the shear lag model with the relation between the crack density and the electrical resistance of the ITO layer. This model can be utilized to design oxide layers with the desired electromechanical stretchability by modifying the graphene meta-interface.

EXPERIMENTAL SECTION

ITO deposition on a PET substrate and a multilayer graphene/PET structure. An ITO (In: 90 wt%, Sn: 10 wt%) target was used to deposit the ITO layer via off-axis RF magnetron sputtering. The distance between the target and the substrate was 10 cm. The initial vacuum was below 8×10^{-6} Torr, and presputtering was carried out for 5 minutes to remove impurities on surface of the target and stabilize the discharge after heating the target to 120°C. ITO was deposited with an RF power of 125 W and a deposition pressure of 1 mTorr.

Growth of graphene and transfer onto the PET substrate. A 25-μm-thick Cu foil was loaded into a 2-inch quartz tube inside a furnace. The furnace was pumped to 1 mTorr before inserting the gas mixture, and heated to 1020°C for 1 hour with 100 sccm of Ar and 50 sccm of H_2. The Cu foil was annealed with the same conditions for 45 minutes. Methane (CH_4) gas was introduced for 35 min while maintaining the temperature at 1020°C. The furnace was then cooled to 800°C with 100 sccm of Ar and 50 sccm of H_2, and then cooled rapidly to room temperature. Following the growth of the graphene, we fabricated multilayer structures using a direct transfer method,[17] which does not lead to the formation of PMMA residue between the graphene layers. PMMA was coated onto the outermost graphene layer on the Cu foil, and was etched using a 0.1 M ammonium persulfate solution. The PMMA support layer for the graphene was rinsed using DI water for 30 min and transferred onto the graphene, forming a PMMA-coated double-layer graphene on Cu foil. By repeating this technique, we successfully fabricated multi-sheet graphene layers on PET substrates that were free from PMMA contamination.

Electro-mechanical tensile test with optical microscope measurement. *In situ* optical microscope observations were made during the uniaxial tensile tests to investigate the crack generation and propagation in the ITO layers. In this manner, it was possible to investigate the cracks that formed at a given strain without allowing them to close following release of the strain. The lens had a working distance of 19 mm and 20× magnification.

Acknowledgment. This research work was supported by the Internal Research Program (SC1090) from the Korea Institute of Machinery and Materials (KIMM), and the Center for Advanced Meta-Materials (CAMM) funded by the Ministry of Science, ICT and Future Planning as Global Frontier Project (CAMM-No. 2014063700 and 2014063701).

REFERENCES AND NOTES

1. J.-H. Kim and J.-W. Park, *Organic Electronics*, 2013, **14**, 3444-3452.

2. H. U. Li and T. N. Jackson, *Electron Device Letters, IEEE*, 2015, **36**, 35-37.

3. S.-T. Han, Y. Zhou and V. A. L. Roy, *Advanced Materials*, 2013, **25**, 5425-5449.

4. H. K. Park, K. Y. Lee, J. S. Seo, J. A. Jeong, H. K. Kim, D. Choi and S. W. Kim, *Advanced Functional Materials*, 2011, **21**, 1187-1193.

5. R. F. Martins, A. Ahnood, N. Correia, L. M. Pereira, R. Barros, P. M. Barquinha, R. Costa, I. M. Ferreira, A. Nathan and E. E. Fortunato, *Advanced Functional Materials*, 2013, **23**, 2153-2161.

6. J. Lewis, *Materials Today*, 2006, **9**, 38-45.

7. Z.-L. Tseng, Y.-C. Tsai, S. Wu, Y.-D. Juang and S.-Y. Chu, *ECS Journal of Solid State Science and Technology*, 2013, **2**, P16-P19.

8. D. R. Cairns, R. P. Witte II, D. K. Sparacin, S. M. Sachsman, D. C. Paine, G. P. Crawford and R. Newton, *Applied Physics Letters*, 2000, **76**, 1425-1427.

9. K. A. Sierros, N. J. Morris, K. Ramji and D. R. Cairns, *Thin Solid Films*, 2009, **517**, 2590-2595.

10. Z. Chen, B. Cotterell and W. Wang, *Engineering Fracture Mechanics*, 2002, **69**, 597-603.

11. International Electrotechnical Commision (IEC) Standard 62047-22, 2014.

12. E.-H. Kim, C.-W. Yang and J.-W. Park, *Journal of Applied Physics*, 2011, **109**, 043511-043511-043518.

13. H. K. Lin, S. M. Chiu, T. P. Cho and J. C. Huang, *Materials Letters*, 2013, **113**, 182-185.

14. C. Peng, Z. Jia, H. Neilson, T. Li and J. Lou, *Advanced Engineering Materials*, 2013, **15**, 250-256.

15. G.-H. Lee, J. Yun, S. Lee, Y. Jeong, J.-H. Jung and S.-H. Cho, *Thin Solid Films*, 2010, **518**, 3075-3080.

16. D.-H. Kim, Y.-S. Kim, J. Wu, Z. Liu, J. Song, H.-S. Kim, Y. Y. Huang, K.-C. Hwang and J. A. Rogers, *Advanced Materials*, 2009, **21**, 3703-3707.

17. S.-K. Lee, B. J. Kim, H. Jang, S. C. Yoon, C. Lee, B. H. Hong, J. A. Rogers, J. H. Cho and J.-H. Ahn, *Nano letters*, 2011, **11**, 4642-4646.

18. H.-J. Choi, S.-G. Yoon, J.-H. Lee and J.-Y. Lee, *ECS Journal of Solid State Science and Technology*, 2012, **1**, Q106-Q109.

19. J.-W. Park, G. Kim, S.-H. Lee, E.-H. Kim and G.-H. Lee, *Surface and Coatings Technology*, 2010, **205**, 915-921.

20. D. R. Cairns and G. P. Crawford, *Proceedings of the IEEE*, 2005, **93**, 1451-1458.

21. X. F. Zhu, B. Zhang, J. Gao and G. P. Zhang, *Scripta Materialia*, 2009, **60**, 178-181.

22. R. M. Niu, G. Liu, C. Wang, G. Zhang, X. D. Ding and J. Sun, *Applied Physics Letters*, 2007, **90**, 161907.

23. C.-H. Hsueh, *J Mater Sci*, 1990, **25**, 4080-4086.

24. H. Tang, B. Foran and D. C. Martin, *Polymer Engineering & Science*, 2001, **41**, 440-448.

25. S. Won, Y. Hwangbo, S.-K. Lee, K.-S. Kim, K.-S. Kim, S.-M. Lee, H.-J. Lee, J.-H. Ahn, J.-H. Kim and S.-B. Lee, *Nanoscale*, 2014, **6**, 6057-6064.

26. X. Liang, M. Tian-Bao, H. Yuan-Zhong and W. Hui, *Nanotechnology*, 2011, **22**, 285708.

27. M. Yanaka, Y. Tsukahara, N. Nakaso and N. Takeda, *J Mater Sci*, 1998, **33**, 2111-2119.

28. H. L. Cox, *British Journal of Applied Physics*, 1952, **3**, 72.

29. J.-Y. Sun, N. Lu, J. Yoon, K.-H. Oh, Z. Suo and J. J. Vlassak, *Journal of Materials Research*, 2009, **24**, 3338-3342.

30. Y. Leterrier, L. Boogh, J. Andersons and J. A. E. Månson, *Journal of Polymer Science Part B: Polymer Physics*, 1997, **35**, 1449-1461.

31. A. Kelly and W. R. Tyson, *Journal of the Mechanics and Physics of Solids*, 1965, **13**, 329-350.

32. A. P. McGuigan, G. A. D. Briggs, V. M. Burlakov, M. Yanaka and Y. Tsukahara, *Thin Solid Films*, 2003, **424**, 219-223.

33. Q. Li, C. Lee, R. W. Carpick and J. Hone, *physica status solidi (b)*, 2010, **247**, 2909-2914.

34. Y. Shen and H. Wu, *Applied Physics Letters*, 2012, **100**, 101909.

35. G. Savini, Y. J. Dappe, S. Öberg, J. C. Charlier, M. I. Katsnelson and A. Fasolino, *Carbon*, 2011, **49**, 62-69.

36. Y. Zhang, C. Wang, Y. Cheng and Y. Xiang, *Carbon*, 2011, **49**, 4511-4517.

37. A. Mora, K. Khan and T. El Sayed, *Electron. Mater. Lett.*, 2014, **10**, 1033-1037.

38. R. K. A. Al-Rub and G. Z. Voyiadjis, *International Journal of Solids and Structures*, 2003, **40**, 2611-2643.

39. A. Mora, K. A. Khan and T. El Sayed, *International Journal of Damage Mechanics*, 2014, DOI: 10.1177/1056789514539362.

FIGURES

(a)

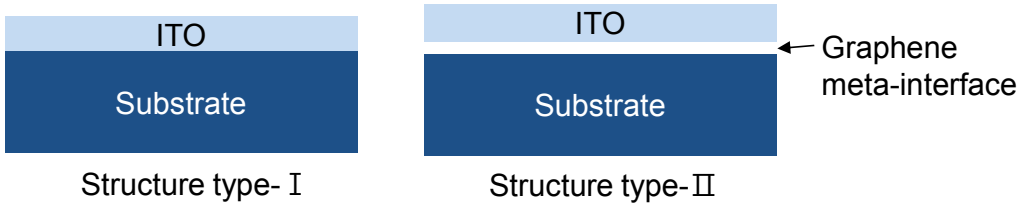

(b)

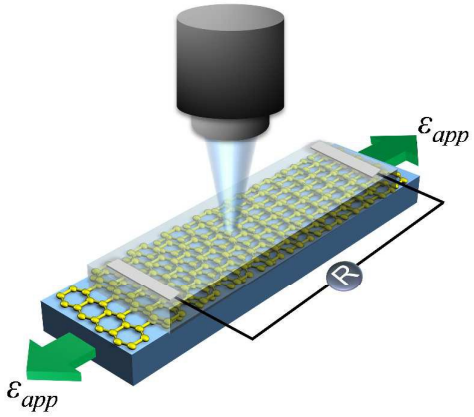

(c)

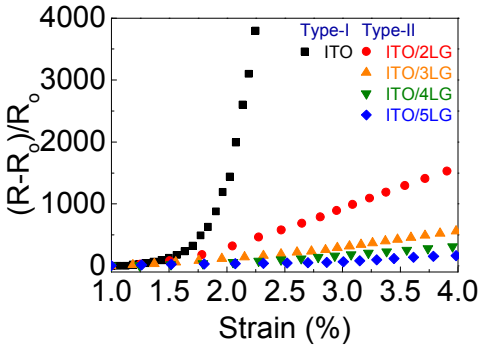

(d)

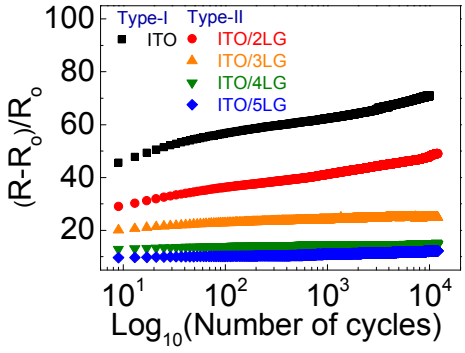

(e)

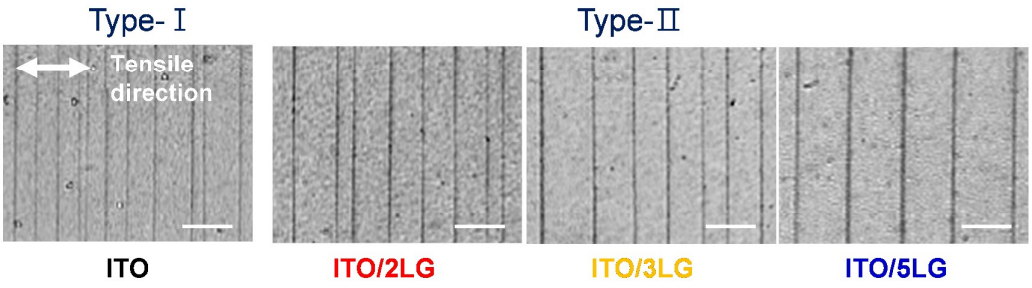

(f)

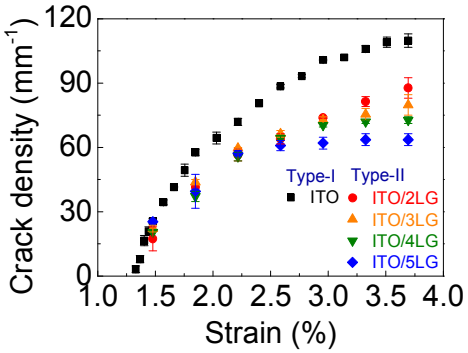

Figure 1. Electromechanical behavior of the type-I and type-II structures as a function of strain. a) Schematic diagrams showing the type-I (ITO/PET) and a type-II (ITO/multilayer graphene (MLG)/PET) structures. b) A schematic diagram of the electromechanical tensile tester with the *in situ* optical microscope observation. c) The normalized electrical resistance of the type-I and type-II structures as a function of the tensile strain. d) Variation of the normalized electrical resistances of type-I and type-II structures under cyclic loading. e) Optical microscope images of the type-I and type-II structures with tensile strain of 3%. The scale bar shows 20 μm. f) The crack densities for the type-I and type-II structures as a function of the strain.

(a)

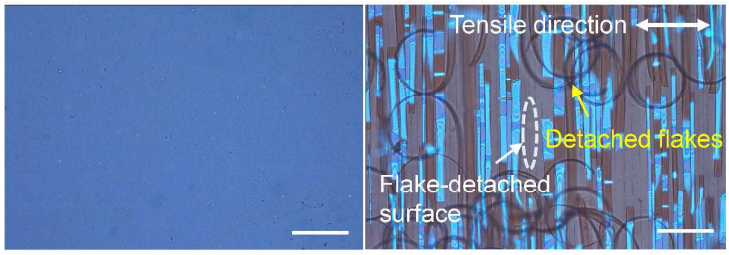

(b)

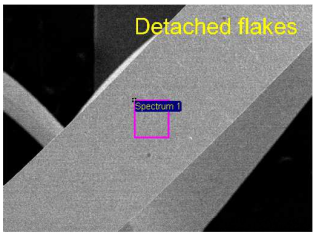

Element	Weight (%)	Atomic (%)
C	8.72	22.16
O	32.22	61.51
In	47.29	12.58
Sn	10.91	2.81

(c)

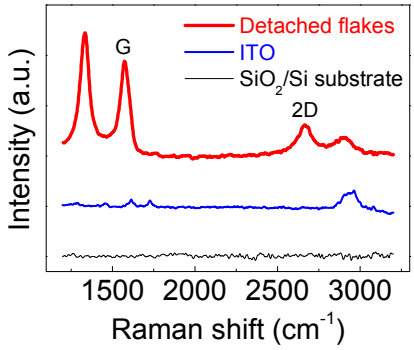

(d)

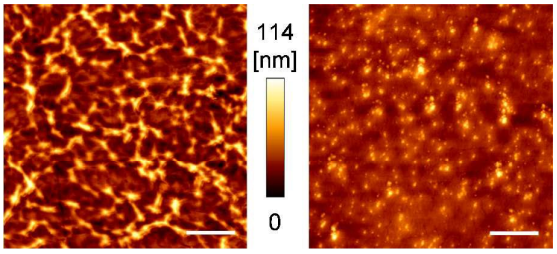

(e)

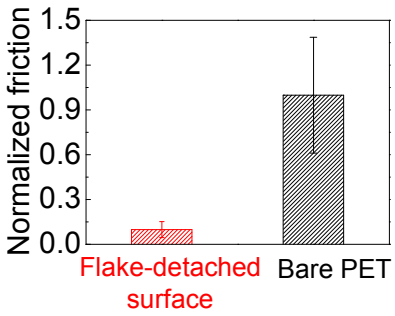

(f)

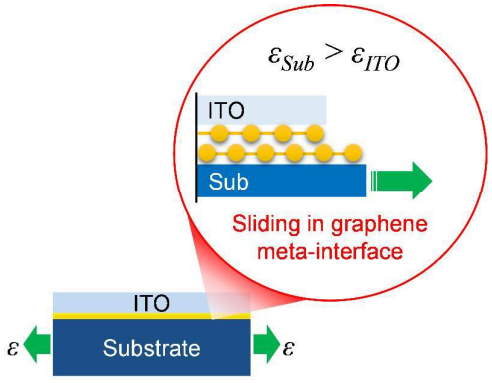

Figure 2. Surface analysis of the ITO/2LG structure after the tensile test to identify the weak interface. a) Optical microscope images of the ITO/2LG structure before and after the tensile test. The scale bar shows 100 μm. b) A SEM image and elemental analysis of a flake detached from the ITO/2LG structure. c) Raman spectrum of a flake detached from the ITO/2LG structure. d) AFM images of the flake-detached surface on an ITO/2LG sample and the surface of a bare PET substrate. The scale bar shows 2 μm. e) The normalized friction of the flake-detached PET surface and the bare PET surface. f) A schematic diagram of the sliding in graphene meta-interface of ITO/2LG structure.

(a)

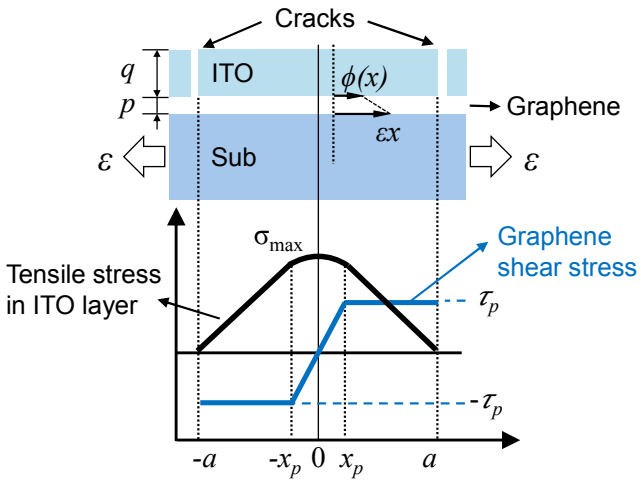

(b)

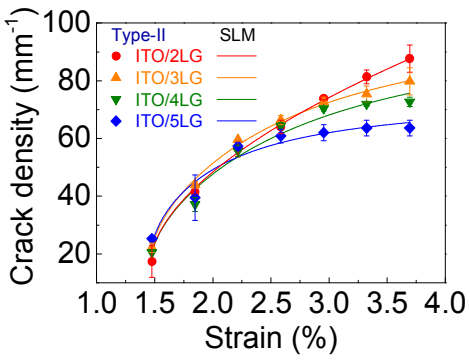

Figure 3. Interlayer behavior of the ITO/MLG (type-II structures). a) A schematic diagram of a cross-section through the ITO/MLG, which consisted of an ITO layer with multiple graphene layers on a PET substrate. b) The crack density as a function of strain (the solid lines were obtained using the shear lag model (SLM), the symbols are the experimentally measured data) for a number of ITO/MLG structures with different numbers of graphene layers.

(a)

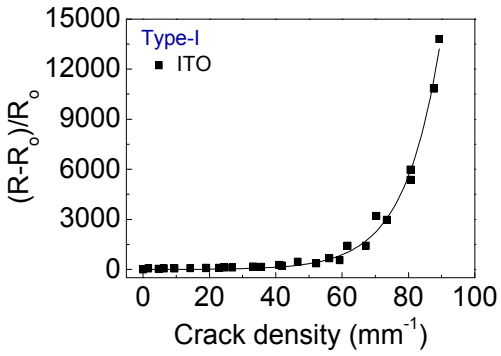

(b)

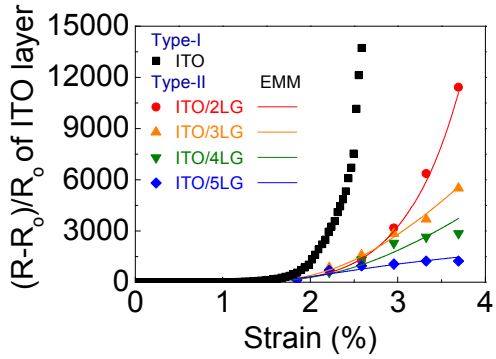

Figure 4. Electromechanical behavior of only the ITO layer in the type-I and type-II structures. a) The relation between the crack density and electrical resistance of the type-I structure. b) The normalized electrical resistance of only the ITO layer in the type-I and type-II structures as a function of the strain. The solid lines show the electromechanical model (EMM) for type-II structures.

Table 1. The parameters of the shear lag model to describe the crack density of the type-II structures.

Samples	p [nm]	q [nm]	σ^*/E	G/E	γ_p
ITO/2LG	0.69	150	0.01445	3.71×10^{-6}	-
ITO/3LG	1.035			6.45×10^{-6}	72.51
ITO/4LG	1.38			7.30×10^{-6}	62.29
ITO/5LG	1.725			1.21×10^{-5}	27.09